

Effect of Processing Parameters on Plastic Flow and Defect Formation in Friction-Stir-Welded Aluminum Alloy



X.H. ZENG, P. XUE, D. WANG, D.R. NI, B.L. XIAO, and Z.Y. MA

The effect of processing parameters on material flow and defect formation during friction stir welding (FSW) was investigated on 6.0-mm-thick 2014Al-T6 rolled plates with an artificially thickened oxide layer on the butt surface as the marker material. It was found that the “S” line in the stir zone (SZ) rotated with the pin and stayed on the retreating side (RS) and advancing side (AS) at low and high heat inputs, respectively. When the tool rotation rate was extremely low, the oxide layer under the pin moved to the RS first and then to the AS perpendicular to the welding direction, rather than rotating with the pin. The material flow was driven by the shear stresses produced by the forces at the pin–workpiece interface. With increases of the rotation rate, the depth of the shoulder-affected zone (SAZ) first decreased and then increased due to the decreasing shoulder friction force and increasing heat input. Insufficient material flow appeared in the whole of the SZ at low rotation rates and in the bottom of the SZ at high rotation rates, resulting in the formation of the “S” line. The extremely inadequate material flow is the reason for the lack of penetration and the kissing bonds in the bottom of the SZ at extremely low and low rotation rates, respectively.

<https://doi.org/10.1007/s11661-018-4615-2>

© The Minerals, Metals & Materials Society and ASM International 2018

I. INTRODUCTION

SINCE its invention in 1991 by the Welding Institute, friction stir welding (FSW) has received much attention from both industry and academia.^[1] Nowadays, FSW has been successfully applied in the aerospace, ship manufacturing, and rail transport industries.^[2–4] Compared with traditional fusion welding, FSW is considered to be an energy efficient, environmentally friendly, and versatile joining technology.^[3–5] Although FSW has found great success, there are still some technical issues. The joint performance is greatly affected by welding defects.^[6,7] Various welding defects such as voids and kissing bonds—weak interfacial bonds that are present when the materials are in intimate contact—may be produced in the welding process if inappropriate FSW parameters are used.

It is well accepted that the macroscopic structure of the FSW joints, welding defects, and characteristic microstructures, such as the “S” line (explained next) and onion rings [the circular or semi-circular bands in the stir zone (SZ)], are controlled by the material flow in the FSW process.^[8] So improving the understanding of how the key factors affect the material flow, microstructural evolution, and defect formation is important for the control and optimization of the quality of weldment.^[9]

However, due to the instantaneity and complexity of the FSW process, there has been no unanimous understanding of the material flow until now. For example, Heurtier *et al.*^[10] reported that the material flow during FSW was composed of circumventing motion, torsional motion, and vortex motion. On the other hand, Schneider *et al.*^[11] suggested that the material flow in FSW was composed of rigid body rotation, uniform translation, and ring cortex. Clearly, the material flow during FSW still needs further investigation.

Usually, welding parameters (rotation rate and traverse speed) are considered as the primary factor affecting the material flow during FSW.^[12,13] For most FSW joints, the morphologies of the SZs change from basin shape to elliptical shape with increasing rotation rate, and a hierarchical-shaped SZ can be observed at very high rotation rates.^[14] Arbegast^[8] pointed out that the welding parameters affected the flow partitioning and the volume of material flowing through the different

X.H. ZENG is with the Shenyang National Laboratory for Materials Science, Institute of Metal Research, Chinese Academy of Sciences, Shenyang, 110016, P.R. China and also with the University of Chinese Academy of Sciences, Beijing, 100049, China. P. XUE, D. WANG, D.R. NI, B.L. XIAO, and Z.Y. MA are with the Shenyang National Laboratory for Materials Science, Institute of Metal Research, Chinese Academy of Sciences. Contact e-mails: pxue@imr.ac.cn and zyma@imr.ac.cn

Manuscript submitted April 23, 2017.

Article published online April 17, 2018

zones of the SZ during FSW of an aluminum alloy. Meanwhile, Xu *et al.*^[15] and Pan *et al.*^[16] found that the spacing of the bands on the longitudinal and horizontal cross-sections, which were in the form of an onion ring structure on the transverse cross-section, was equal to the distance traveled by the welding tool in one revolution.

Although these studies mentioned the relationship between material flow and welding parameters, the effect of welding parameters on the material flow has not been elucidated clearly. Furthermore, little attention has been paid to the material flow in the bottom of the SZ under different welding parameters, which influences the formation of bottom defects including lack of penetration and kissing bonds. Optimization of parameters is usually achieved by the trial and error method, which would be more cost effective if a thorough understanding of the effect of welding parameters on the plastic deformation and material flow were to be established.

In recent years, tracer technology has been widely used to study the material flow during FSW.^[17–23] One of the tracer technologies uses additional marker materials. Various marker materials such as steel balls,^[17] tungsten balls,^[18] pure aluminum sheets,^[19] aluminum alloy sheets,^[15] and pure copper foils^[20] are inserted into the welded workpieces at different locations to trace the material flow. Based on the displacement of the marker materials, some useful information about the material flow during FSW has been obtained. However, there are intrinsic differences between the marker materials and the base materials, which can lead to relative movement near the interface. Thus, it is difficult to determine the real flow behavior of the base materials during FSW using additional marker materials.

Another important tracer technique is based on FSW of dissimilar materials, where the contrast between different types of corrosion by dissimilar materials indicates the material flow.^[21–23] Similarly to the additional marker materials, however, the different flow capacities between dissimilar materials may bring out unreliable information on the material flow. Therefore, better tracer technologies are still needed to study the real material flow of the FSW process.

The “S” line, also called the “lazy S” or “zigzag” line, is usually observed in the SZ of the FSW joints of Al alloys, especially when low heat-input parameters are used.^[24,25] It has been proven that the formation of the “S” line is due to the breaking and redistribution of the initial oxide layer on the butt surfaces during the FSW process.^[26] Thus, the oxide layer on the butt surface should be a good marker material to show the material flow during FSW.

However, it should be pointed out that the inherent oxide layer on the Al plate is too thin, making it harder to track. In order to overcome the deficiency of a natural oxide layer, Zhang *et al.*^[27] produced an extraneous oxide layer on the butting surface of the plate by sectioning the plate using electric discharge machining (EDM). Compared with the conventional marker materials, the artificial oxide layer is not only thin but also metallurgically bonded with the workpiece. The results of this study showed that the “S” line gradually became

more and more intact as the welding speed was increased from 100 to 400 mm/min.

In this study, the oxide layer, thickened artificially on the butt surface of the Al alloy plate, was used as the marker material to investigate the material flow during FSW. The effect of the welding parameters on the material flow and defect formation during FSW was examined in detail. An analytical model is proposed to explain material flow during FSW.

II. EXPERIMENTAL PROCEDURE

The material used in this study was a 6.0-mm-thick 2014Al-T6 rolled plate. An artificially thickened oxide layer on the butt surface (hereafter referred to as the oxide layer) was obtained by EDM. Plates with a length of 370 mm and a width of 65 mm were butt welded along the rolling direction with a tool tilt angle of 2.7 deg using an FSW machine (China FSW Center, Beijing, China). The welding tool used in this study was made of heat-treated tool steel with a shoulder diameter of 20 mm and a pin diameter of 8 mm with a length of 5.73 mm (threaded taper pin with a pin thread space of 1.0 mm). The plunge depth of the shoulder was 0.2 mm during FSW.

To understand the effect of the welding parameters on the material flow during FSW, the 2014Al-T6 plates were welded with different FSW parameters, which are shown in Table I. These different FSW parameters were defined as 200-100 to 1000-100 for a constant traverse speed and 800-100 to 800-400 for a constant tool rotation rate, respectively.

All the samples used for the metallographic analysis were cross-sectioned from the joints perpendicular to the welding direction. After grinding and polishing, the samples were etched by two kinds of reagents. One is a modified Keller’s etching reagent which includes 2 mL of HF, 3 mL of HCl, 5 mL of HNO₃, and 190 mL of H₂O. A high-quality image of the grain structure can be obtained after using this etching reagent. The other is 2 pct NaOH solution, and the characteristic microstructure related to the oxide layer, such as the “S” line and onion rings, can be observed clearly after using this etching reagent. All etched samples were observed through an optical microscope (OM, HC-300Z/OL, Olympus Corporation).

Table I. Welding Parameters of FSW 2014Al-T6 Joints

Rotation Rate (rpm)	Traverse Speed (mm/min)	Designation
200	100	200–100
400		400–100
500		500–100
800		800–100
1000		1000–100
800	200	800–200
	400	800–400
	600	800–600

III. RESULTS

A. Macrostructures of FSW Joints

Figure 1 shows the cross-sectional metallographs of the FSW 2014Al-T6 joints under different welding parameters etched by Keller's reagent. It can be observed that different macroscopic morphologies were obtained in the FSW 2014Al-T6 joints under various welding parameters. With the increase of the rotation rate, the macrostructures of the SZs changed from basin shape to elliptical shape and a hierarchical SZ was clearly observed at the highest rotation rate of 1000 rpm in this study. However, the shapes of the SZs did not change obviously with the increase of traverse speed under a constant rotation rate. For example, all the SZs exhibited elliptical shapes when the rotation rate was 800 rpm.

It is well known that the deformed grains in the thermo-mechanically affected zone (TMAZ) can reveal some important information about material flow during FSW. Under a very low rotation rate of 200 rpm (Figure 2(a)), the area of the TMAZ was very small and it was very difficult for material flow and plastic deformation to occur in the TMAZ at both the advancing side (AS) and the retreating side (RS). As the rotation rate was increased to 800 rpm, the middle and top materials in the TMAZ moved upward while the movement of the bottom material showed a downward trend (Figures 2(b) and (c)). When the rotation rate was increased to 1000 rpm, the SZ was divided into two parts and a part of material in the TMAZ flowed

into the boundary zone between these two parts (Figure 2(d)).

For the cross-sectional macrostructures of the FSW samples under different traverse speeds (Figures 1(d) and (f) through (h)), almost the same material flow trends were achieved in the TMAZ, where the middle and top material moved upward and the bottom material moved downward. Thus, the increase of the rotation rate can enhance the material flow and plastic deformation, and the rotation rate has a more significant influence on the TMAZ material flow compared with the traverse speed.

B. The Evolution of the "S" Line

Figure 3 shows the cross-sectional metallographs of the FSW 2014Al-T6 joints under different welding parameters etched by NaOH solution. A dark line (continuous or discontinuous) can be observed in the center region of the SZ, winding down from the top workpiece surface, through the weld region, to the bottom of the SZ, which is the so-called "S" line. Meanwhile, the bottom oxide layer is almost intact without effective joining under the SZ at low rotation rates (Figures 3(a) and (b)). Thus, the "S" line together with the bottom oxide layer can be considered to be the boundary between the AS and the RS material.

Figures 3(a) through (e) show the evolution of the "S" line in the FSW joints under different rotation rates. According to the SZ shapes and the "S" line distributions, the FSW joints are of four types, determined by

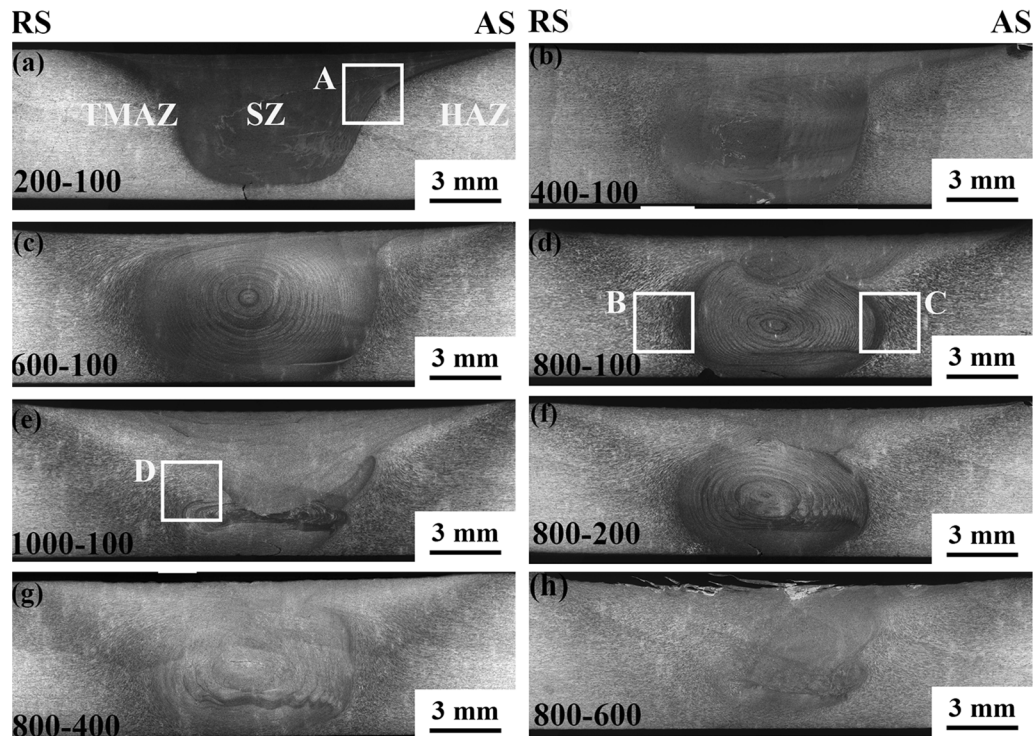


Fig. 1—Metallograph of cross-sections under different welding parameters etched by Keller's reagent: (a) 200-100, (b) 400-100, (c) 600-100, (d) 800-100, (e) 1000-100, (f) 800-200, (g) 800-400, (h) 800-600.

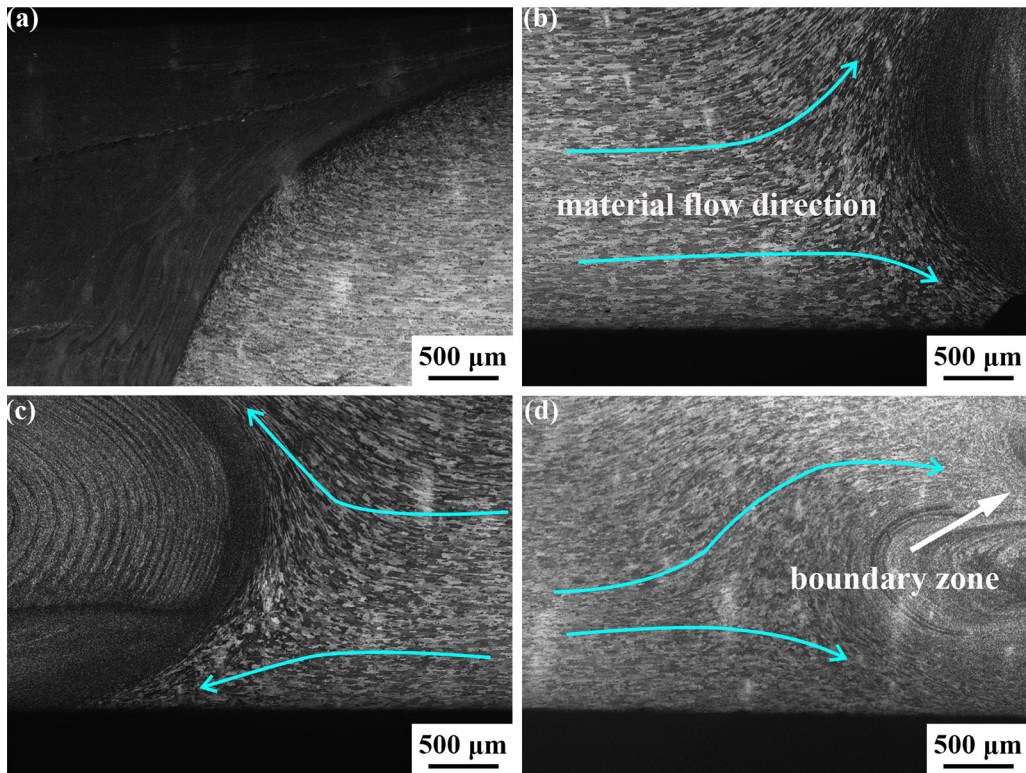


Fig. 2—Material flow direction in TMAZ under different welding parameters: (a) Position A, (b) Position B, (c) Position C, (d) Position D.

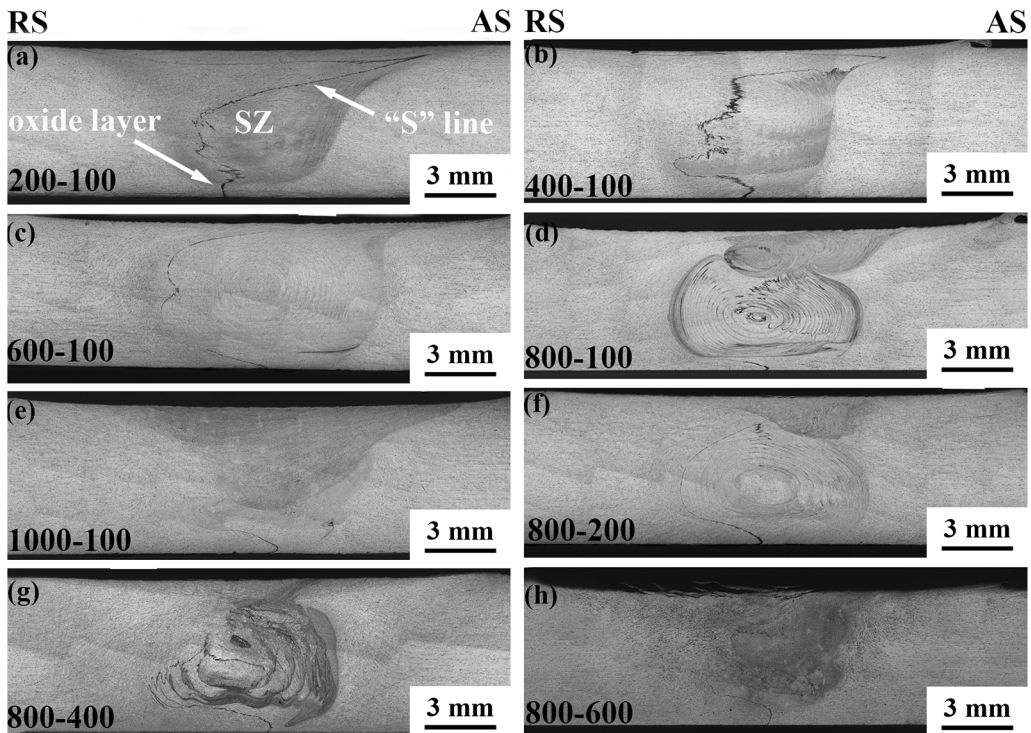


Fig. 3—Metallograph of cross-sections under different welding parameters etched by NaOH solution: (a) 200-100, (b) 400-100, (c) 600-100, (d) 800-100, (e) 1000-100, (f) 800-200, (g) 800-400, (h) 800-600.

the rotation rate used: extremely low (200 rpm), low (400 to 500 rpm), moderate (800 rpm), or high (1000 rpm). Under the extremely low or low rotation rate, the “S” line started from the top surface near the RS of the SZ and extended to the bottom surface near the weld centerline, exhibiting a continuous curve. In the top workpiece surface and the bottom region of the SZ, the AS material passed the weld centerline and pushed the material to the RS. In contrast, the RS material passed the weld centerline and pushed the material to the AS in the upper middle region of the SZ. As the rotation rate was increased to a moderate value of 800 rpm, onion rings structure appeared in the SZ and the “S” line along the edge of onion rings region was discontinuous and was often dragged into the onion rings region, where it mixed with the rings (Figure 3(d)). At a high rotation rate of 1000 rpm, the SZ divided into two parts and the “S” line was only observed in the bottom and along the interface between the SZ and TMAZ (Figure 3(e)).

Figures 3(d) and (f) through (h) show the effect of the traverse speed on the evolution of the “S” line in the FSW joints under a constant rotation rate of 800 rpm. Some interesting results could be obtained from these microstructural observations. First, the “S” line was discontinuous, and no obvious “S” line characteristic could be observed in the top region of the SZs, indicating that the AS material was fully mixed with the RS material. Second, onion rings structure did not form in the SZ of the 800-600 sample, and the movement

of the “S” line was not severe (Figure 3(h)). Third, with the decrease of the traverse speed, a well-developed onion rings structure appeared in the SZ and the “S” line was dragged into the onion rings region and mixed with the rings. Clearly, both high rotation rate and low traverse speed were beneficial for the mixing of material during FSW.

C. Defect Formation During FSW

Figure 4 shows the morphologies of the oxide layers and the “S” lines at the bottom of the SZs under different welding parameters. All the oxide layers and “S” lines were continuous, which indicated that the material flow at the bottom was not very severe. Under a very low rotation rate of 200 rpm (Figure 4(a)), the oxide layer in the bottom of the workpiece did not move with the pin. Therefore, a lack of penetration was observed in the bottom of the 200-100 sample. As the rotation rate was increased to 400 rpm (Figure 4(b)), the oxide layer at the bottom moved into the AS and the kissing bonds could be observed at the bottom of the 400-100 sample. With the increase of the rotation rate to 500 rpm (Figure 4(c)), the “S” line at the bottom started to move into the RS. When the rotation rate was increased to 1000 rpm, the “S” line at the bottom flowed into the AS (Figure 4(d)). Compared with the 400-100 sample, however, the mixing of the AS and RS material at the bottom of 1000-100 sample was more adequate and no bottom defects were observed in the 500-100 and

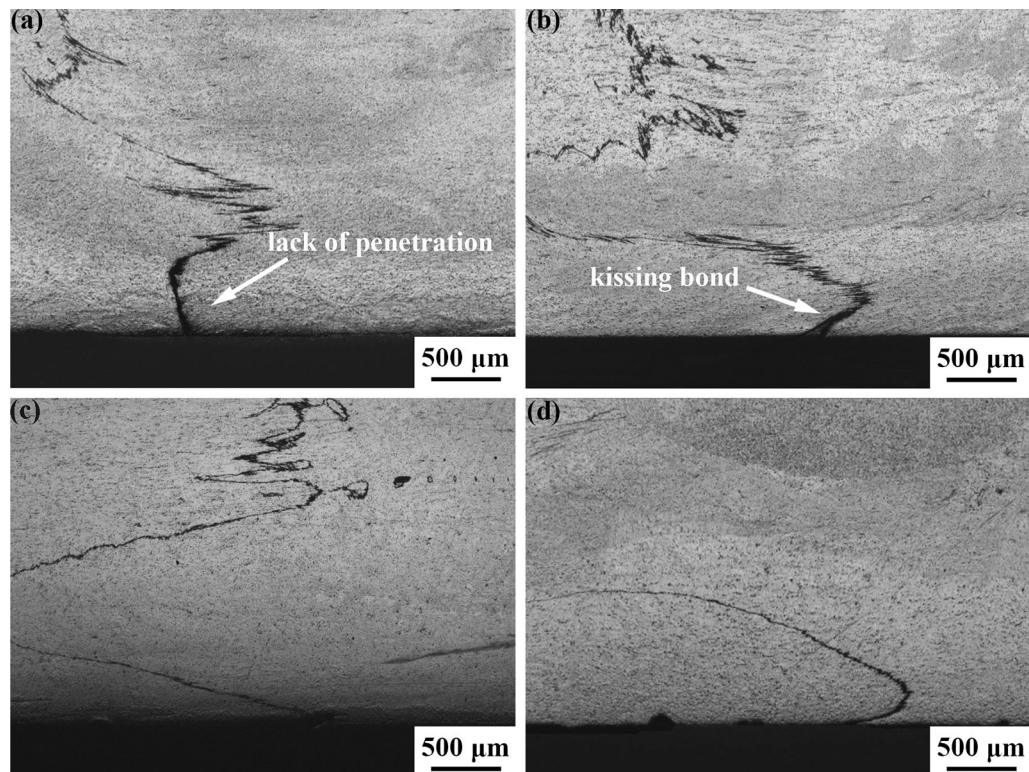


Fig. 4—Metallograph of the bottom material of cross-sections under different welding parameters etched by NaOH solution: (a) 200-100, (b) 400-100, (c) 500-100, (d) 1000-100.

1000-100 samples. Therefore, the increase of the rotation rate was beneficial for eliminating the bottom defects during FSW.

IV. DISCUSSION

A. The Analysis of Stress and Material Flow

Clearly, the whole of the SZ can be divided into three parts,^[13,28] as shown in Figure 5: (a) the shoulder-affected zone (SAZ) in the upper region, where the shoulder affects the material flow; usually, the SAZ is considered to be the wide top region in the basin-shaped SZ^[29]; (b) the pin-affected zone (PAZ) in the middle

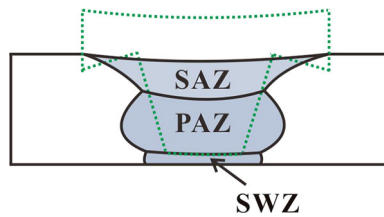


Fig. 5—Schematic diagrams of three parts in the whole of the SZ.

region, where only the pin affects the material flow; and (c) the swirl zone (SWZ) in the bottom region, where the end of the pin affects the material flow.

Based on the results in Figures 3 and 4, there are two types of movement of the “S” line in the SAZ and PAZ and three types of movement in the SWZ, which can be summarized in the schematic diagram in Figure 6. Under a low rotation rate, it is very difficult for the material to flow due to the low heat input, and the “S” lines in the SAZ and PAZ rotate with the pin and stay on the RS (Figure 6(a)). With the increase of the rotation rate, the material flow becomes easier, and the “S” lines in the SAZ and PAZ rotate with the pin and move to the AS (Figure 6(b)). Many investigations of material flow during FSW support this viewpoint.^[14,18,30]

The “S” line in the SWZ rotates with the pin and stays on the RS and AS at the moderate and high rotation rates, respectively, as in the SAZ and PAZ (Figures 6(d) and (e)). When the tool rotation rate is low (e.g., 400 rpm), it is very difficult for the material to flow in the bottom of the SZ. The oxide layer moves first to the RS and then to the AS perpendicular to the welding direction, rather than rotating with the pin (Figure 6(c)). Because the temperature of the material behind the pin is higher than that in front of the pin,^[31,32] the material

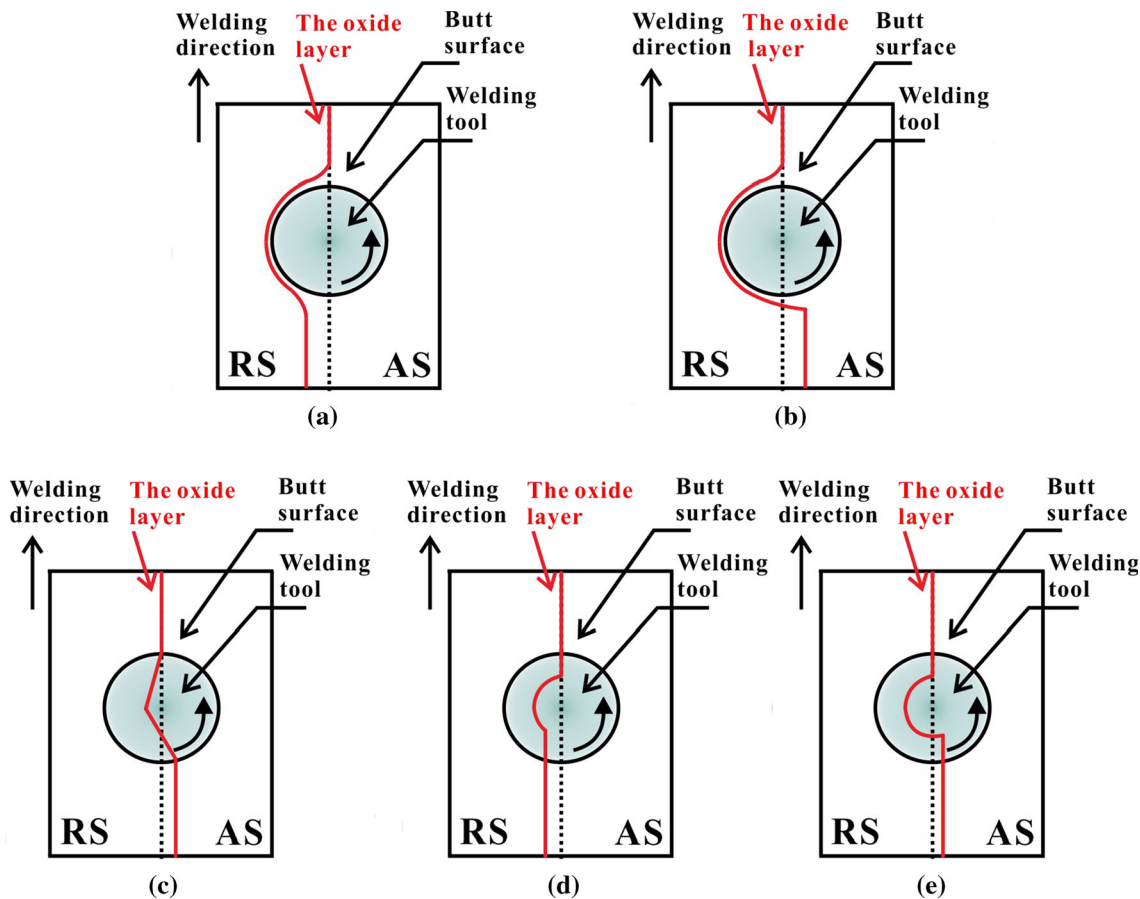


Fig. 6—Schematic diagrams of the movement types of the “S” line: (a, b) the “S” line in SAZ and PAZ; (c to e) the “S” line and oxide layer in the SWZ.

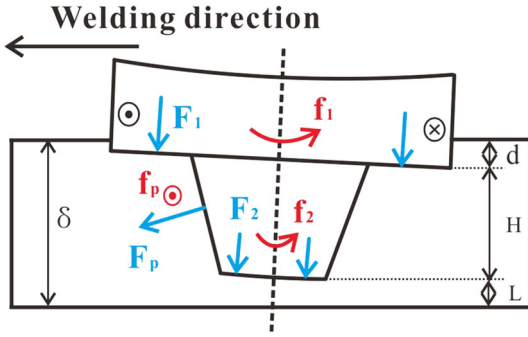


Fig. 7—Schematic diagram of analysis of forces during FSW.

flow behind the pin is better than that in the front of pin, and finally the oxide layer in the SWZ stays on the AS.

The forces at the pin–workpiece interface have a considerable influence on the material flow during FSW^[33] and these forces are illustrated schematically in Figure 7. Due to the plunge of the shoulder, two downward forces (F_1 and F_2) act on the material in the upper and lower zones of the workpiece, which are produced by the shoulder and pin, respectively. Meanwhile, there is relative movement between the tool and the workpiece; the friction forces act on the material (f_1 and f_2) and their directions are the same as the direction of tool rotation. Due to the forward motion of the pin, the high positive force and friction force act on the workpiece (F_p and f_p). The above friction forces (f_1 , f_2 , and f_p) between the welding tool and the workpiece result in a high shear stress on the material adjacent to the pin with a direction from the AS to the RS.

Due to the relative movement between the tool and the workpiece, the friction force produced by the shoulder is given by

$$f_1 = \mu F_1, \quad [1]$$

where F_1 is the downward force produced by the shoulder, which decreases with increasing rotation rate and decreasing traverse speed,^[34,35] and μ is the friction coefficient, which is given by^[36,37]

$$\mu = 0.5 \times \exp(-\delta\omega r) \quad [2]$$

$$\delta = 0.31 \times \exp\left(\frac{\omega r}{1.87}\right) - 0.026 \quad [3]$$

where δ is a dimensionless slip coefficient, ω is the rotation rate, and r is the radial distance from the tool axis. Equations [2] and [3] are reported to be valid for ωr ranging between 0.1 and 1.6 ms^{-1} .^[37] Generally, the FSW parameters used in Al alloys are within this range. Meanwhile, the friction coefficient decreases with the increase of the rotation rate according to Eqs. [2] and [3]. Thus, the friction force produced by the shoulder decreases with the increase of the rotation rate.

Under the assumption that the plastic deformation of Al alloys is a kind of high viscosity, incompressible non-Newtonian fluid,^[19,31] the material flow during FSW is considered to be a kind of lamellar flow.

Because of the internal friction, the shear stress produced by the friction force decreases with increasing material thickness. Assuming that the decrease of shear stress is linear, the shear stress produced by the shoulder can be calculated as

$$\tau_1 = \frac{f_1}{S_1} - M\eta L, \quad [4]$$

where S_1 is the area of the material under the shoulder, M is a constant related to the materials intrinsic properties, L is the thickness of the material under the shoulder, and η is the kinematic viscosity.

When removing the shoulder shear stress, according to Eq. [4], the material thickness (L), which is influenced by the shoulder, is given by

$$L = \frac{f_1}{S_1 M \eta}. \quad [5]$$

During the steady welding process, the mechanical balance of the tool can be represented by

$$F_2 \cos \theta + F_p \sin \alpha = F_1 \cos \theta, \quad [6]$$

where F_2 is the downward force produced by the pin, α is the cone angle of the pin, and θ is the tilt angle of the tool during FSW. Thus, the downward force produced by the pin lateral is given by

$$F_p = \frac{\cos \theta}{\sin \alpha} (F_1 - F_2). \quad [7]$$

The shear stress produced by the friction force in the pin lateral is given by

$$\tau_p = \frac{f_p}{S_p} - M\eta L, \quad [8]$$

where f_p is the friction force produced by the pin lateral, S_p is the area of the pin lateral, and l is the thickness of the material which flows with the pin.

Under a very low rotation rate, the shear stress produced by the forces at the pin–workpiece interface is smaller than the shear strength of the material at a relatively low temperature, so the material cannot move with the welding tool in the SZ. However, the shear strength of the material decreases considerably in the SZ under a high rotation rate due to the increased temperature and is smaller than the shear stress produced by the forces at the pin–workpiece interface, so the material can flow easily and moves with the welding tool in the SZ.^[33]

Further, during the steady welding process, the stress state of the material in the upper and middle regions can be obtained (Figures 8(a) and (b)). If $L \leq \frac{f_1}{S_1 M \eta}$, the shear stresses are produced by both the shoulder and the pin lateral (τ_1 and τ_p , Figure 8(a)). This means that the material flow in the upper region of the workpiece is affected by the shoulder and pin. This part of the material forms the SAZ. If $L > \frac{f_1}{S_1 M \eta}$, the shear stress is produced only by the pin lateral (Figure 8(b)). This

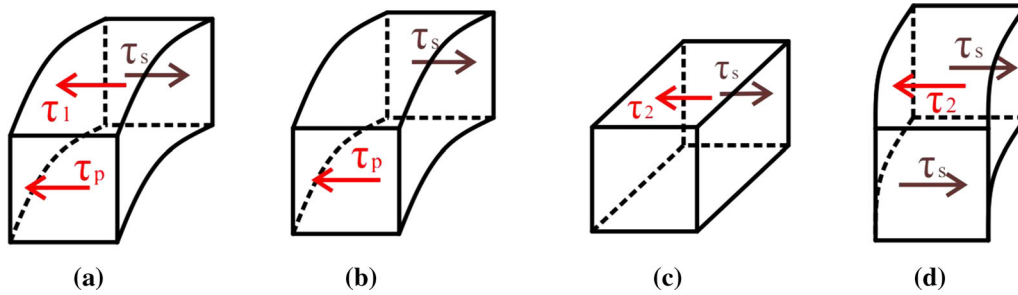


Fig. 8—Schematic diagram of stress analysis of different locations: (a) SAZ, (b) PAZ, (c) SWZ under low rotation rate, (d) SWZ under moderate and high rotation rates.

means that the material flow in the middle region of the workpiece is mainly affected by the pin and this part of the material forms the PAZ.

The friction force in the SWZ and the shear stress produced by the pin are similar to the friction forces in the SAZ and PAZ and the shear stress produced by the shoulder, respectively. Therefore, the shear stress produced by the pin is given by

$$\tau_2 = \frac{f_2}{S_2} - M\eta L_P, \quad [9]$$

where S_2 is the area of the material under the pin and L_P is the thickness of the material under the pin, which is affected by the pin shear stress. Similarly to the friction force produced by the shoulder, the friction force produced by the pin decreases with the increase of the rotation rate.

Usually, the static friction force achieved between the workpiece and the workbench is relatively low during the normal FSW process. Thus, it can be ignored in this study. As the material in the SWZ moves first to the RS and then to the AS (Figure 6(c)), the flow resistance, which is the material's shear strength (Figure 8(c)), comes from the material in front of the pin. According to Eq. [9], the thickness of the bottom material which flows with the pin is given by

$$L_{P1} = \frac{f_2 - \tau_s S_2}{M\eta S_2}. \quad [10]$$

When the material in the SWZ rotates with the pin (Figure 5(d) or (e)), the flow resistance, which is double the material shear strength (Figure 7(d)), comes from the material in front of and behind the pin. According to Eq. [9], the thickness of the bottom material which flows with the pin is given by

$$L_{P2} = \frac{f_2 - 2\tau_s S_2}{M\eta S_2}. \quad [11]$$

B. The Evolution of the Welding Butt Surface

The material flow can be reflected from the evolution of the “S” line originating from the welding butt surface. Based on the results in Figures 3 and 4, the evolution of

the “S” line under different rotation rates can be described using the schematic diagrams shown in Figure 9. In order to conveniently describe the evolution of the welding butt surface, the “S” line is defined as part I to part VI from the top to the bottom of the SZ, respectively, and the bottom oxide layer is defined as part X in the 200-100 and 400-100 samples. As can be seen in Figure 9(a), under a very low rotation rate of 200 rpm, a continuous and curved “S” line is observed in the SZ, which is related to the forces at the tool–workpiece interface during FSW. The “S” line in the upper SAZ moves to the RS due to the shoulder friction force (f_1). It is very hard for the material to flow due to the very low heat input at the low rotation rate, and the “S” line in the upper SAZ rotates with the tool and finally stays at the RS (point A in Figure 9(a)).

Along the thickness direction, the material is driven by both the shoulder friction force (f_1) and the pin lateral friction force (f_p). Therefore, the material can move around the pin and stay on the AS (point B in Figure 9(a)), forming Part I of the “S” line. The friction force produced by the shoulder decreases with the distance from the top surface along the thickness direction of the workpiece.^[38] The friction force produced by the shoulder disappears at Point C, and Part II of the “S” line is produced between points B and C. Thus, the depth of the SAZ is from the top of the SZ to point C, which is larger than the depth of the wide top region in the basin-shaped SZ. This result is different from those of other researchers.^[29] The material in Part III of the “S” line is only affected by the pin lateral friction (f_p), so the shape of Part III of the “S” line is less curly. Meanwhile, the formation of Part V of the “S” line is related to the shape of the bottom of the pin. Due to the extremely low rotation rate, it is very difficult for the material to flow, and the oxide layer (Part X) does not move with the pin.

In the low rotation rate state (Figure 9(b)), although the driving force decreases, the heat input and temperature increase and the material flow becomes easier during FSW.^[39] Points B and C move up and Part III of the “S” line moves to the weld center line. The depth of the SAZ is equal to that of the wide top region in the basin-shaped SZ. It is clear that the depth of the SAZ decreases with the increase of the rotation rate due to the reduced shoulder friction force. Meanwhile, the material in the PAZ moves to the RS adequately and

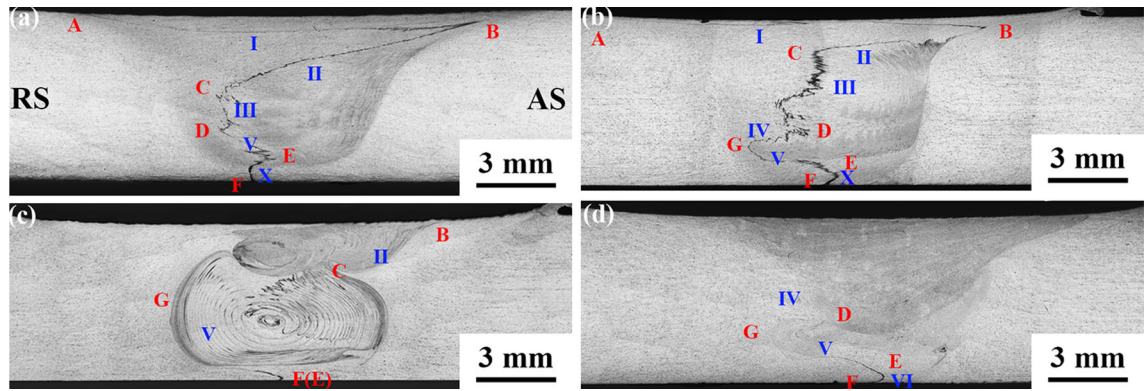


Fig. 9—Schematic diagram of joint surface evolution with rotation rate analysis: (a) extremely low rotation rate, (b) low rotation rate, (c) moderate rotation rate, (d) high rotation rate.

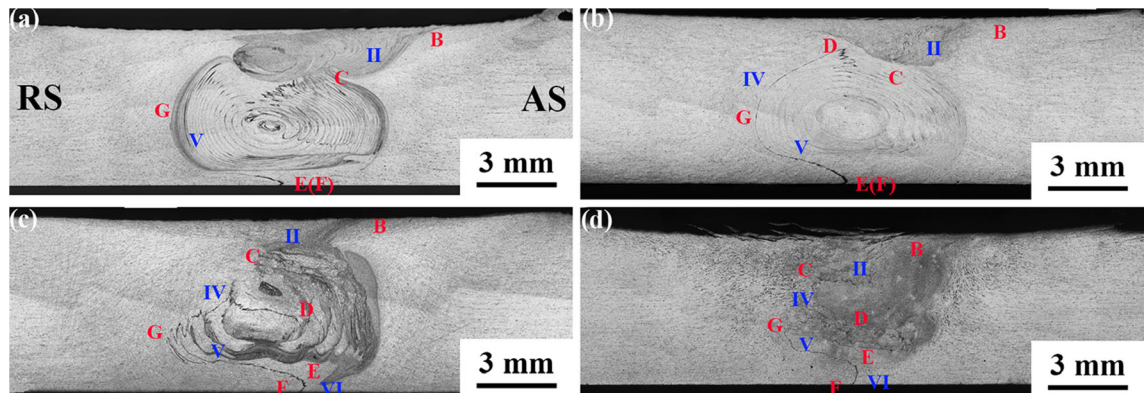


Fig. 10—Schematic diagram of joint surface evolution with welding speed analysis: (a) extremely low welding speed, (b) low welding speed, (c) moderate welding speed, (d) high welding speed.

Part IV of the “S” line is produced. Because of the increased heat input, point E and the oxide layer (Part X) in the SWZ move to the AS but cannot rotate with the pin and finally stay on the AS.

In the moderate rotation rate state (Figure 9(c)), the material flow becomes easier due to the increased heat input. Point A moves from the RS to the AS and point B moves upwards. Points A and B overlap and Part I of the “S” line disappears. The increase of the rotation rate leads to severe material flow in the vertical direction, so the material flow at the upper part of the SZ in the AS can break the “S” line, resulting in a short Part II of the “S” line. At the same time, the material flow at the middle of the SZ can break Part IV of the “S” line. The SZ has a well-developed onion rings and point G moves upwards toward the RS. Xu *et al.*^[15] also observed a similar phenomenon. Meanwhile, the material in the SWZ can rotate with the pin and finally stay on the RS.

At a high rotation rate (Figure 9(d)), the higher heat input enhances the material flow and gives rise to a larger depth of the SAZ. Compared with other welding conditions, the depth of the SAZ under a high rotation rate is the largest. Thus, with the increase of the tool rotation rate, the depth of the SAZ first decreases and

then increases. At the same time, only Parts IV and VI of the “S” line can be observed in the bottom of the SZ and the material in the SWZ can rotate with the pin and finally stay on the AS.

The evolution of the “S” line under different traverse speeds can be described using the schematic diagrams in Figure 10. According to Eqs. [2] and [3], the driving force of the material flow depends on the material’s position and the tool rotation rate. However, the traverse speed affects the welding heat input which controls the material flow. With the increase of the traverse speed, the heat input and the material flow decrease. When the traverse speed is 100 or 200 mm/min, a well-developed onion rings structure appears in the SZ and the “S” line merges into the onion rings region (Figures 10(a) and (b)). At a moderate or high traverse speed (Figures 10(c) and (d)), Point D and Part IV of the “S” line move downward and the material in the SWZ cannot rotate with the pin and stay on the AS (Part VI of the “S” line). The thickness of each layer in the onion rings structure decreases with the increase of the traverse speed. Moreover, because of the high welding speed, the material cannot move fast enough and there is no onion rings structure in the SZ.

C. Analysis of the Mechanism of Welding Defect Formation

The “S” line was formed through the fragmentation and dispersion of the oxide layer from the initial butt surface under the pin’s stirring action during FSW.^[24,26] At relatively low rotation rates (200 to 500 rpm), the material flow is not strong enough to break up the oxide layer. The oxide layer is continuously distributed throughout the SZ. Thus, the continuous “S” line is only observed in the cross-section of the SZ at low rotation rates (Figures 3(a) and (b)). The present result is comparable with those obtained by other investigators.^[24,26] Under a high rotation rate, according to the force and material flow analyses during the FSW process, the material flow is very weak at the bottom of the SZ and the oxide layer cannot be broken up in this zone. Thus, insufficient material flow is the reason for the formation of the “S” line at the low rotation rate and the bottom of the SZ at high rotation rates.

Because of the weak material flow under a low rotation rate, bottom defects including a lack of penetration and kissing bonds can be produced at the bottom of the SZ and the material thickness under the pin (Figure 7) is given by

$$L_B = \delta - H - H_\delta, \quad [12]$$

where δ is the thickness of the workpiece, H is the pin length, and H_δ is the plunge depth of the shoulder. The abovementioned results and analyses can be summarized as follows: (a) when $L_{P1} < L_B$, the bottom material does not flow with the welding tool, and the lack of penetration occurs in the bottom of the SZ in this case (Figure 4(a)); (b) when $L_{P2} < L_B < L_{P1}$, the bottom material moves first to the RS and then to the AS perpendicular to the welding direction, rather than rotating with the tool (Figure 6(c)), and the kissing bonds defect forms in the bottom of the SZ (Figure 6(b)); (c) when, the bottom material rotates with the pin and stays in the RS or the AS (Figures 6(d) and (e)), and there is no defect in the bottom of the SZ. These results can be used to choose the appropriate pin length and plunge depth to avoid the bottom defects during FSW.

V. CONCLUSIONS

In this study, the material flow and defect formation during FSW were investigated in detail by a marker material of the artificially thickened oxide layer and the conclusions drawn from the results can be summarized as follows:

1. Increasing the rotation rate can enhance the material flow and plastic deformation in the TMAZ.
2. The morphologies of the SAZ vary with the FSW parameters. Under a very low rotation rate (200 rpm), the depth of the SAZ is from the top of the SZ to point C, which is larger than the depth of the wide top region in the basin-shaped SZ. With increasing tool rotation rate, the depth of the SAZ

first decreases and then increases due to the decreasing shoulder friction force and increasing heat input.

3. The evolution of the welding butt surface is dependent on the FSW parameters. The “S” lines in the SZ rotate with the pin and stay on the RS and AS at low and high heat inputs, respectively. Under an extremely low rotation rate of 200 rpm, the oxide layer in the SWZ does not move with the welding tool, and the lack of penetration occurs in the bottom of the SZ. When the rotation rate increases to 400 rpm, the oxide layer in the SWZ moves to the RS first and then to the AS perpendicular to the welding direction, rather than rotating with the pin, and the kissing bonds form in the bottom of the SZ.
4. Based on the experimental observations and the forces at the pin–workpiece interface during FSW, the insufficient material flow, which is the reason for the formation of the “S” line, appears in the whole of the SZ at low rotation rates and in the bottom of the SZ at high rotation rates. Moreover, the extremely inadequate material flow is the reason for the lack of penetration and the kissing bonds in the bottom of the SZ at extremely low and low rotation rates, respectively.

ACKNOWLEDGMENT

This work was supported by the National Natural Science Foundation of China under Grant No. 51331008.

REFERENCES

1. W.M. Thomas, E.D. Nicholas, J.C. Needham, M.G. Murch, P. Templesmith, and C.J. Dawes, G.B. Patent Application No.9125978.8, 1991.
2. R.S. Mishra and Z.Y. Ma: *Mater. Sci. Eng. R*, 2005, vol. 50, pp. 1–78.
3. S. Ji, Z. Li, Z. Zhou, and B. Wu: *J. Mater. Eng. Perform.*, 2017, vol. 26, pp. 5085–96.
4. Z.Y. Ma: *Metall. Mater. Trans. A*, 2008, vol. 39A, pp. 642–58.
5. D. Zhemchuzhnikova, S. Mironov, and R. Kaibyshev: *Metall. Mater. Trans. A*, 2016, vol. 48A, pp. 150–58.
6. X.C. Liu and C.S. Wu: *Mater. Des.*, 2016, vol. 90, pp. 350–58.
7. Y. Tao, Z. Zhang, D.R. Ni, D. Wang, B.L. Xiao, and Z.Y. Ma: *Mater. Sci. Eng. A*, 2014, vol. 612, pp. 236–45.
8. W.J. Arbegast: *Scr. Mater.*, 2008, vol. 58, pp. 372–76.
9. Z. Zhu, M. Wang, H. Zhang, X. Zhang, T. Yu, and Z. Wu: *Metals*, 2017, vol. 7, pp. 256–571.
10. P. Heurtier, M.J. Jonesb, C. Desrayauda, J.H. Driver, F. Montheillet, and D. Allehaux: *J. Mater. Process. Technol.*, 2006, vol. 171, pp. 348–57.
11. J.A. Schneider and A.C. Nunes: *Metall. Mater. Trans. B*, 2004, vol. 35B, pp. 777–83.
12. F. Simoes and D.M. Rodrigues: *Mater. Des.*, 2014, vol. 59, pp. 344–51.
13. Z. Zhang, B.L. Xiao, D. Wang, and Z.Y. Ma: *Metall. Mater. Trans. A*, 2010, vol. 42A, pp. 1717–26.
14. J.H. Yan, M.A. Sutton, and A.P. Reynolds: *Sci. Technol. Weld. Join.*, 2005, vol. 10, pp. 725–36.
15. S.W. Xu and X.M. Deng: *Acta Mater.*, 2008, vol. 56, pp. 1326–41.
16. Y. Pan and D.A. Lados: *Metall. Mater. Trans. A*, 2017, vol. 48A, pp. 1708–26.
17. K. Colligan: *Weld. J.*, 1999, vol. 78, pp. 229–37.

18. Y. Morisada, H. Fujii, Y. Kawahito, K. Nakata, and M. Tanaka: *Scr. Mater.*, 2011, vol. 65, pp. 1085–88.
19. X.C. Liu, C.S. Wu, and G.K. Padhy: *Scr. Mater.*, 2015, vol. 102, pp. 95–98.
20. H.N.B. Schmidt, T.L. Dickerson, and J.H. Hattel: *Acta Mater.*, 2006, vol. 54, pp. 1199–1209.
21. P. Pourahmad, M. Abbasi, and T. Nonferr: *Metal. Soc.*, 2013, vol. 23, pp. 1253–61.
22. Y. Shimoda, M. Tsubaki, T. Yasui, M. Fukumoto, T. Fujita, and J. Osawa: *Steel. Res. Int.*, 2010, vol. 81, pp. 1108–11.
23. M. Fukumoto, M. Tsubaki, T. Yasui, and K. Miyagawa: *Steel. Res. Int.*, 2010, vol. 81, pp. 1096–99.
24. Y.S. Sato, F. Yamashita, Y. Sugiura, S.H.C. Park, and H. Kokawa: *Scr. Mater.*, 2004, vol. 50, pp. 365–69.
25. S.S. Di, X.Q. Yang, D.P. Fang, and G.H. Luan: *Mater. Chem. Phys.*, 2007, vol. 104, pp. 244–48.
26. Y.S. Sato, H. Takauchi, S.H.C. Park, and H. Kokawa: *Mater. Sci. Eng. A*, 2005, vol. 405, pp. 333–38.
27. Z. Zhang, B.L. Xiao, and Z.Y. Ma: *Metall. Mater. Trans. A*, 2013, vol. 44A, pp. 4081–97.
28. Z. Zhang, B.L. Xiao, and Z.Y. Ma: *Mater. Sci. Eng. A*, 2005, vol. 614, pp. 6–15.
29. K. Ramanjaneyulu, G.M. Reddy, and A.V. Rao: *Trans. Indian Inst. Met.*, 2014, vol. 67, pp. 769–80.
30. A.K. Kadian and P. Biswas: *J. Mater. Eng. Perform.*, 2015, vol. 24, pp. 4119–27.
31. A.K. Kadian and P. Biswas: *J. Manuf. Process.*, 2017, vol. 26, pp. 382–92.
32. Z. Zhang and H.W. Zhang: *J. Mater. Process. Technol.*, 2009, vol. 209, pp. 241–70.
33. Z.W. Chen, T.P. Sang, and Y. Qi: *Mater. Sci. Eng. A*, 2008, vol. 474, pp. 312–16.
34. D.K. Yaduwanshi, S. Bag, and S. Pal: *Mater. Des.*, 2016, vol. 92, pp. 166–83.
35. Y.C. Lin, J.J. Liu, and J.N. Chen: *Exp. Mech.*, 2013, vol. 53, pp. 1573–82.
36. M. Mehta, K. Chatterjee, and A. De: *Sci. Technol. Weld. Joining*, 2013, vol. 18, pp. 191–97.
37. Q. Li and M. Lovell: *J. Mater. Process. Technol.*, 2005, vol. 160, pp. 245–56.
38. Z.Y. Ma, S.R. Sharma, and R.S. Mishra: *Mater. Sci. Eng. A*, 2006, vol. 422, pp. 269–78.
39. X.X. Zhang, B.L. Xiao, and Z.Y. Ma: *Metall. Mater. Trans. A*, 2011, vol. 42A, pp. 3218–28.